*J. Fluid Mech.* (1976), *vol.* 76, *part* 2, *pp.* 363–381
*Printed in Great Britain*



# A moving-wall boundary layer with reverse flow

By J. B. KLEMP
National Center for Atmospheric Research, Boulder, Colorado
AND ANDREAS ACRIVOS
Department of Chemical Engineering, Stanford University,
Stanford, California 94305

(Received 26 February 1976)

The problem of uniform flow past a flat plate whose surface has a constant velocity $\lambda U$ opposite in direction to that of the mainstream is considered for large values of the Reynolds number $R$. In a previous communication (Klemp & Acrivos 1972) it was shown that, if the region of reverse flow which is established next to the plate as a consequence of its motion is $O(R^{-\frac{1}{2}})$ in thickness, the appropriate laminar boundary-layer equations have a solution provided $\lambda \leqslant 0{\cdot}3541$. Here the analysis is extended to the range $\lambda > 0{\cdot}3541$, which cannot be treated using a conventional boundary-layer approach. Specifically, it is found that for $\lambda > 0{\cdot}3541$ the flow consists of three overlapping domains: (*a*) the external uniform flow; (*b*) a conventional boundary layer with reverse flow for $x_s < x < 1$, where $x_s$ refers to the point of detachment of the $\psi = 0$ streamline and $x = 1$ is the trailing edge of the plate; and (*c*) an inviscid collision region in the neighbourhood of $x_s$, having dimensions $O(R^{-\frac{1}{2}})$ in both the streamwise and the normal direction, within which the reverse moving stream collides with the uniform flow, turns around and then proceeds downstream. It is established furthermore that $x_s = 0$ for $0 \leqslant \lambda \leqslant 1$ and that $x_s < 0$ for $\lambda > 1$.

Also, detailed streamline patterns were obtained numerically for various $\lambda$'s in the range of $0 < \lambda \leqslant 2$ using a novel computational scheme which was found to be more efficient than that previously reported. Interestingly enough, the drag first decreased with $\lambda$, reached a minimum at $\lambda = 0{\cdot}3541$, and then increased monotonically until, at $\lambda = 2$, it was found to have attained essentially the value predicted from the asymptotic $\lambda \to \infty$ similarity solution available in the literature. Thus it is felt that the present numerical results plus the two similarity solutions for $\lambda = 0$ and for $\lambda \to \infty$ fully describe the high-$R$ steady flow for all non-negative values of $\lambda$.

## 1. Introduction

Steady laminar flows at high Reynolds numbers $R$ containing regions of reverse flow constitute an important class of viscous flow problems for which, in general, a quantitative theoretical description is still lacking. For example, when separation occurs in the flow past a solid body, the surface streamline ($\psi = 0$) no longer conforms to the body contour beyond the point of detachment, with the result

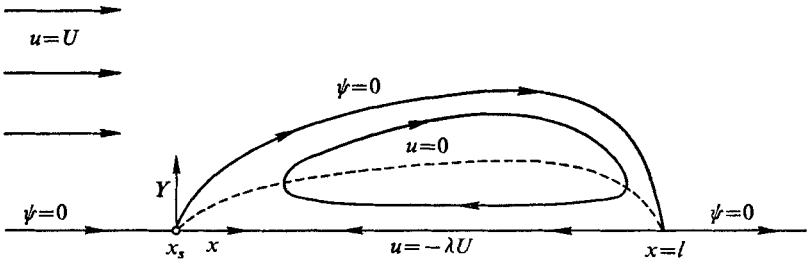


FIGURE 1. A sketch of the region of closed streamlines for a plate with a reverse moving surface.

that conventional methods of boundary-layer analysis no longer apply. This is especially true wherever, as is often the case, the surface streamline is displaced an order-one distance from the body downstream of separation, since the external flow thereby encounters an effective body whose geometry is *a priori* unknown.

In what follows, we shall consider the admittedly rarer situation in which the region of reverse flow is confined within an $O(R^{-\frac{1}{2}})$ distance from the solid body. This case is of course much simpler to analyse since the structure of the inviscid flow remains unaffected, to a first approximation, by the presence of separation. Consequently, the pressure that is impressed on the boundary layer by the external flow can be determined over the whole length of the body surface (excluding locally singular regions) on the basis of a conventional inviscid analysis for flow past the given body contour.

The particular problem on which we shall focus our attention is depicted in figure 1 and involves the high Reynolds number uniform flow past a stationary flat plate of finite length $l$ whose surface has a constant velocity $\lambda U$ opposite in direction to that of the mainstream. ($U$ is the velocity of the undisturbed flow and $R \equiv Ul/\nu$ is the Reynolds number, with $\nu$ being the kinematic viscosity of the fluid.) We shall seek to determine the steady flow pattern when $R \gg 1$, on the assumption, based on the numerical solutions of the full Navier–Stokes equations by Leal & Acrivos (1969), that the region of reverse flow remains within an $O(R^{-\frac{1}{2}})$ distance from the plate. In other words, we shall be dealing here with a moving-wall boundary-layer problem with zero pressure gradient, which, incidentally, has a variety of physical applications, e.g. in the extrusion of plastics.

In a previous communication (Klemp & Acrivos 1972, henceforth denoted by I), numerical solutions to the boundary-layer equations were presented for values of the dimensionless surface speed $\lambda$ in the range $0 < \lambda \leqslant 0{\cdot}3541$. (Here $\lambda$ replaces the variable $\epsilon$ in I since our analysis will not be restricted to small values of this parameter.) For the cases considered in I, detachment and reattachment of the $\psi = 0$ streamline took place at the leading and at the trailing edge of the plate, respectively, and, as expected, the thickness of the region of reverse flow increased monotonically with $\lambda$. Also, in this range of $\lambda$, the total drag decreased monotonically.

A significant feature of the analysis developed in I is that near the leading

edge, i.e. as $x \to 0^+$, the boundary-layer equations reduce via a similarity transformation to the familiar Blasius equation

$$2F''' + FF'' = 0, \tag{1.1a}$$

with boundary conditions

$$F(0) = 0, \quad F'(0) = -\lambda, \quad F'(\infty) = 1. \tag{1.1b}$$

Surprisingly, solutions to the above were found to exist only for $\lambda \leqslant \lambda^* \equiv 0{\cdot}3541$, and hence the scheme developed in I failed when $\lambda$ exceeded that 'critical' value $\lambda^*$.

This failure to obtain solutions to the boundary-layer equations for $\lambda > \lambda^*$ could be explained, of course, by supposing that viscous effects are no longer confined to a thin, $O(R^{-\frac{1}{2}})$ layer adjacent to the plate. Nevertheless, we do recall that when $\lambda \to \infty$, or alternatively when the plate surface velocity is kept fixed but the stream speed is reduced to zero, a solution of boundary-layer type still exists (cf. Sakiadis 1960) in which the boundary layer grows upstream, starting from the trailing edge. In fact, the boundary-layer equations again reduce to (1.1*a*) but with boundary conditions

$$F(0) = 0, \quad F'(0) = 1, \quad F'(\infty) = 0.$$

Consequently it seems reasonable to suppose that the boundary-layer simplifications would apply for intermediate values of $\lambda$ given that they are known to remain valid for $\lambda \leqslant \lambda^*$ and $\lambda \gg 1$. Further support is provided for this argument by the numerical solutions in I, which reveal no rapid increase in the boundary-layer thickness as $\lambda \to \lambda^*$.

The approach which we shall presently pursue assumes that the failure to obtain a solution for $\lambda > \lambda^*$ results not from the breakdown of the boundary-layer approximations over the length of the plate, but rather from the fact that the flow near the leading edge does not conform to the similarity transformation leading to (1.1). Of course, if the similarity transformation is not valid immediately downstream of the point of detachment $x = x_s$, the boundary-layer approximations inherent in (1.1) must also cease to apply in the vicinity of $x_s$. With this in mind, we shall develop solutions for $\lambda > \lambda^*$ in which the conventional boundary-layer structure is altered by the presence of an inviscid region surrounding the point of detachment and having $O(R^{-\frac{1}{2}})$ dimensions in both the streamwise and the normal direction. Within this inviscid domain the mainstream collides with the reverse flow which is returning along the surface of the plate. The colliding streams are then deflected away from the plate and, in the process, the reverse flow is turned and leaves the inviscid region in the mainstream direction. The dividing streamline remains within an $O(R^{-\frac{1}{2}})$ distance from the plate and thus the boundary-layer equations apply downstream of $x_s$. In the present investigation the entire flow structure will be described in detail. Also, it will be demonstrated that appropriate solutions exist in each region and that the required matching conditions between regions are satisfied.

In seeking solutions valid over the entire range $0 < \lambda < \infty$, we re-emphasize that, as mentioned earlier, the boundary layer extends indefinitely far upstream in the limit $\lambda \to \infty$. For this reason, if $1 \ll \lambda < \infty$, one would certainly expect that

the reverse flow would carry enough momentum to penetrate upstream of the leading edge. This implies, of course, that the point of detachment would then lie at some $x \equiv x_s < 0$. Indeed, we shall show in what follows that a self-consistent analysis can be developed along these lines which allows us to determine the steady flow for $R \gg 1$ over the whole spectrum of values of the parameter $\lambda$.

Before proceeding with this new analysis for dealing with the case $\lambda > \lambda^*$, we shall re-examine in the next section the solution in the range $0 < \lambda \leqslant \lambda^*$, already considered in I, in order to introduce a different numerical approach for solving the boundary-layer equations with flow reversal which we found to be considerably superior to that presented in I. In §3, we shall reconsider briefly (1.1) and shall show that it admits two solutions for $0 < \lambda \leqslant \lambda^*$ of which only one, however, correctly describes the flow pattern near the leading edge of a finite flat plate. In §4, we shall provide a detailed analysis of the flow structure for $\lambda > \lambda^*$ and finally, in §5, we shall present numerical solutions based on this analysis. Although these solutions apply, of course, only to the moving-wall boundary-layer problem of figure 1, they contain a number of novel features which, it is hoped, may also exist in other high-$R$ steady flow problems involving flow reversal. Thus the present analysis may be of interest within the wider context of boundary-layer flows with separation.

## 2. Solutions for $0 < \lambda \leqslant \lambda^* \equiv 0{\cdot}3541$

When the surface velocity parameter $\lambda$ lies in the range $0 < \lambda \leqslant \lambda^*$, a region of closed streamlines is formed next to the plate (cf. figure 1) in which the surface streamline ($\psi = 0$) detaches at the leading edge ($x = 0$) and reattaches at the trailing edge of the plate. Owing to a discontinuity in the boundary conditions along $y = 0$, the boundary-layer equations become locally singular at these two points, but otherwise, as shown in I, they remain valid throughout the boundary layer. Near the leading edge, this local singularity can be removed by a standard transformation of co-ordinates which takes into account the fact that, as $x \to 0^+$, the flow pattern depicted in figure 1 must be of a self-similar type. Thus, defining

$$\psi(x,y) \equiv (x/R)^{\frac{1}{2}} f(x,y), \quad \eta \equiv Y/x^{\frac{1}{2}}, \quad \text{with } Y \equiv R^{\frac{1}{2}}y, \tag{2.1}$$

we have for the dimensionless form of the boundary-layer equations

$$f_{\eta t} + f_\eta f_{x\eta} - f_x f_{\eta\eta} = (2x)^{-1}\{2f_{\eta\eta\eta} + f f_{\eta\eta}\}, \tag{2.2}$$

with boundary conditions

$$\left.\begin{aligned} &f(x,0,t) = 0, \quad f_\eta(x,\infty,t) = 1 \quad \text{for all} \quad x > 0, \\ &f_\eta(x,0,t) = -\lambda \quad \text{for} \quad 0 \leqslant x \leqslant 1, \quad f_{\eta\eta}(x,0,t) = 0 \quad \text{for} \quad x > 1, \\ &f_\eta(0,\eta,t) = F'(\eta), \quad \text{where } F(\eta) \text{ satisfies (1.1).} \end{aligned}\right\} \tag{2.3}$$

In I, numerical solutions were obtained by solving the steady-state form of (2.2) separately in the forward- and in the reverse-flow portions of the boundary layer by integrating the equations in each domain in the direction of the flow. To generate solutions in this manner required an iterative procedure in which the position of the $u = 0$ curve separating the two regions was adjusted until the

shear stress became continuous across this line. Although this technique produced valid steady-state solutions, there is no unique procedure for adjusting the $u = 0$ curve after each iteration and convergence cannot be rigorously proved. In contrast, we shall obtain solutions here by integrating the time-dependent boundary-layer equations until steady state is achieved. The advantage of this approach is that, since the time-dependent equations are hyperbolic in the streamwise direction, they can be stepped forward in time using centred finite differences for the spatial derivatives in $x$. Thus a finite-difference scheme can be constructed which is stable regardless of the sign of $u$; information is freely transmitted in either direction and an iterative procedure which is based on locating the position of the reverse-flow region is not required.

In solving the time-dependent equation (2.2) an initial condition is needed in addition to the boundary conditions (2.3). This initial condition is, of course, somewhat arbitrary since the primary interest here lies in determining the steady-state solution. An obvious choice is $f_\eta(x, \eta, 0) = 1$ but another possibility is to let

$$f_\eta(x, \eta, 0) = F'(\eta), \tag{2.4}$$

which assumes that the solution to (1.1) applies initially throughout the boundary layer. Both of these initial conditions were tested and found to produce the same steady-state results although convergence to the steady state was achieved much more quickly using (2.4). This to be expected since, as shown in I, the steady-state solution does not deviate substantially from $F(\eta)$ over the forward portion of the plate.

To obtain the finite-difference solution of (2.2)–(2.4), second-order centred differences were used for all spatial derivatives and the equation corresponding to (2.2) was stepped forward in time by means of a leapfrog scheme for the time derivative. Of course, since the coefficient multiplying the right-hand side of (2.2) tends to infinity as $x \to 0$, an explicit scheme would have required a prohibitively small time step in order to satisfy the linear stability criterion, and hence (2.2) was solved using an implicit representation for terms containing the $\eta$ derivatives. Specifically, with $u \equiv f_\eta$ being the variable which was actually stepped forward in time, (2.2) was recast into the finite-difference form

$$\left.\begin{aligned} \delta_{2t} u + u\delta_{2x} u = (2x)^{-1}\{2\delta_{\eta\eta}\bar{u}^{2t} + (f + 2x\delta_{2x} f)\delta_{2\eta}\bar{u}^{2t}\}, \\ \delta_\eta f = \bar{u}^\eta, \end{aligned}\right\} \tag{2.5}$$

with initial and boundary conditions

$$\left.\begin{aligned} u(x, \eta, 0) = F'(\eta), \quad f(x, 0, t) = 0, \quad u(x, L, t) = 1, \\ u(x, 0, t) = -\lambda \quad \text{for} \quad 0 \leqslant x \leqslant 1, \quad u_\eta(x, 0, t) = 0 \quad \text{for} \quad x > 1. \end{aligned}\right\} \tag{2.6}$$

Here, the difference operators are defined by

$$\left.\begin{aligned} \bar{\phi}^{n\xi} &= \tfrac{1}{2}\{\phi(\xi + \tfrac{1}{2}n\Delta\xi) + \phi(\xi - \tfrac{1}{2}n\Delta\xi)\}, \\ \delta_{n\xi}\phi(\xi) &= (n\Delta\xi)^{-1}\{\phi(\xi + \tfrac{1}{2}n\Delta\xi) - \phi(\xi - \tfrac{1}{2}n\Delta\xi)\}, \\ \delta_{\xi\xi}\phi(\xi) &= (\Delta\xi)^{-2}\{\phi(\xi + \Delta\xi) - 2\phi(\xi) + \phi(\xi - \Delta\xi)\}, \end{aligned}\right\} \tag{2.7}$$

with $\phi$ being the appropriate dependent variable, $\xi$ the independent variable and $n\Delta\xi$ the number of grid intervals over which the operation takes place.

The downstream boundary $x = x_B$ was located five grid points beyond the trailing edge of the plate. Here, the $x$ derivatives were replaced by one-sided difference operators and, to maintain stability, the boundary value in the $\partial u/\partial x$ term was time averaged (Elvius & Sundström 1973), such that

$$\partial u(x_B, \eta, t)/\partial x = (\Delta x)^{-1}\{\tfrac{1}{2}[u(x_B, \eta, t+\Delta t) + u(x_B, \eta, t-\Delta t)] - u(x_B - \Delta x, \eta, t)\}. \quad (2.8)$$

Also, the value of $L$ in (2.6) was kept fixed at 6, after establishing that test runs with $L = 6$ and $L = 10$ gave nearly identical results, and the grid intervals $\Delta x$ and $\Delta\eta$ were set equal to 0·02 and 0·1, respectively. Furthermore, to ensure linear stability for disturbances propagating in the $x$ direction, $\Delta t$ was fixed at $2{\cdot}5 \times 10^{-3}$. In this way, convergence of the numerical solution to five decimal places was achieved within a dimensionless time of about 5.

In order to suppress the growth of nonlinear instabilities, a small damping term proportional to $\partial^2 u/\partial x^2$ was added to (2.5); when written in Dufort–Frankel form (averaging of the middle point in time), this also suppressed the time splitting of the computational mode in the leapfrog scheme. The coefficient of this second derivative was set at about $10^{-3}$, a value which was small enough not to affect the steady-state results in any significant way.

Because of the implicit representation of all the terms involving $\eta$ derivatives in (2.5), all the values of $u$ in a given column had to be determined simultaneously. Thus the equations represented by (2.5) were stepped forward in time by sweeping through the flow field in the $x$ direction and solving implicitly for $u$ at each value of $x$ by inverting a tridiagonal matrix.

The solutions which were obtained by the procedure just described for $\lambda = 0{\cdot}1$, 0·2 and 0·3 were compared with those computed previously and depicted in figures 3 and 4 of I. In all cases, the differences between the two sets of results with regard to such characteristic features of the flow as the thickness of the reverse-flow region, the position of the vortex centre and the associated minimum value of the stream function, the wall shear stress, etc. were less than a few per cent. Such differences were to be expected of course since the steady-state iterative procedure employed in I incorporated a refined mesh near the point of reattachment, but made use of only a first-order-accurate resolution of the $x$ derivatives.

In view of the close agreement between the present solutions and those reported in I, these will not be reproduced here. It is instructive though to consider the flow structure for $\lambda = \lambda^* \equiv 0{\cdot}3541$, the maximum value of the surface velocity parameter for which a solution to (1.1) exists. Figure 2 is a sketch of the closed-streamline region, which is seen to be qualitatively similar, in all respects, to those with lower values of $\lambda$. Indeed there is no evidence to suggest that, if $\lambda$ were to exceed $\lambda^*$ by a very small amount, the thickness of the boundary layer would increase dramatically, or that the boundary-layer simplifications would cease to apply. In fact, it would appear that the only portion of the flow which would

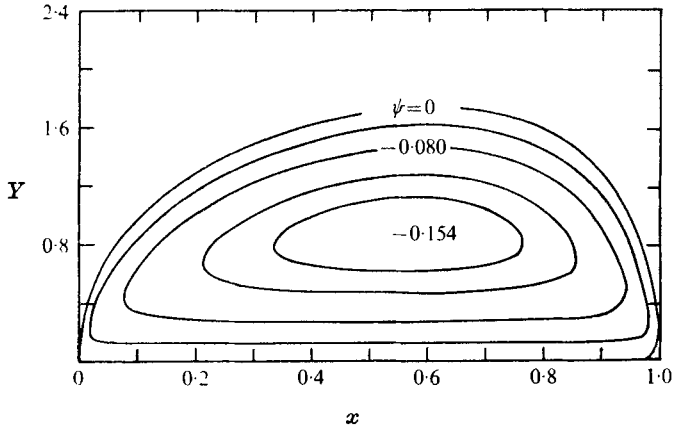


FIGURE 2. The structure of the closed-streamline region when $\lambda = \lambda^* \equiv 0{\cdot}3541$.

suffer a fundamental modification as $\lambda$ exceeded $\lambda^*$ would be that near the leading edge of the plate, where the similarity transformation (2.1) would then no longer hold.

## 3. Re-examination of the similarity solution

Before turning to the case $\lambda > \lambda^*$ we wish to reconsider here briefly certain properties of (1.1), since it is the failure of this system to admit a solution when $\lambda$ exceeds the critical value 0·3541 which appears to be responsible for the fact that the finite-plate problem can no longer be described solely on the basis of the boundary-layer equations when $\lambda > \lambda^*$. Some of the features of the solution for $0 < \lambda \leqslant \lambda^*$ were described previously in I, where a physical justification was given for the observed monotonic decrease in the wall shear stress, proportional to $F''(0)$, with increasing $\lambda$. In the course of the present investigation it was found, however, that the solution discussed in I is not unique and that another perfectly acceptable solution of (1.1) exists for $\lambda$ in the range $0 < \lambda < \lambda^*$.

This second solution was found by solving (1.1) as an initial-value problem (and not as a boundary-value problem as was done in I) with $F''(0)$ as a parameter. The resulting curves of $F'(\infty)$ *vs.* $F''(0)$ for various values of $\lambda$ are plotted in figure 3, from which it is evident that, for each $\lambda$ in the range $0 < \lambda < \lambda^*$, two solutions exist satisfying the boundary condition $F'(\infty) = 1$. It is moreover easy to show that both of these solutions meet the additional requirement that the vorticity, proportional to $F''(\eta)$, should decay exponentially as $\eta \to \infty$. Hence both sets are acceptable solutions to the boundary-layer equations.

Of these two families of solutions, the one described in I as well as by other investigators (Leal & Acrivos 1969; Robillard 1971) corresponds to the larger value of the wall shear stress and, as $\lambda \to 0$, converges uniformly to the Blasius function. This is in contrast to the second solution, for which the boundary-layer

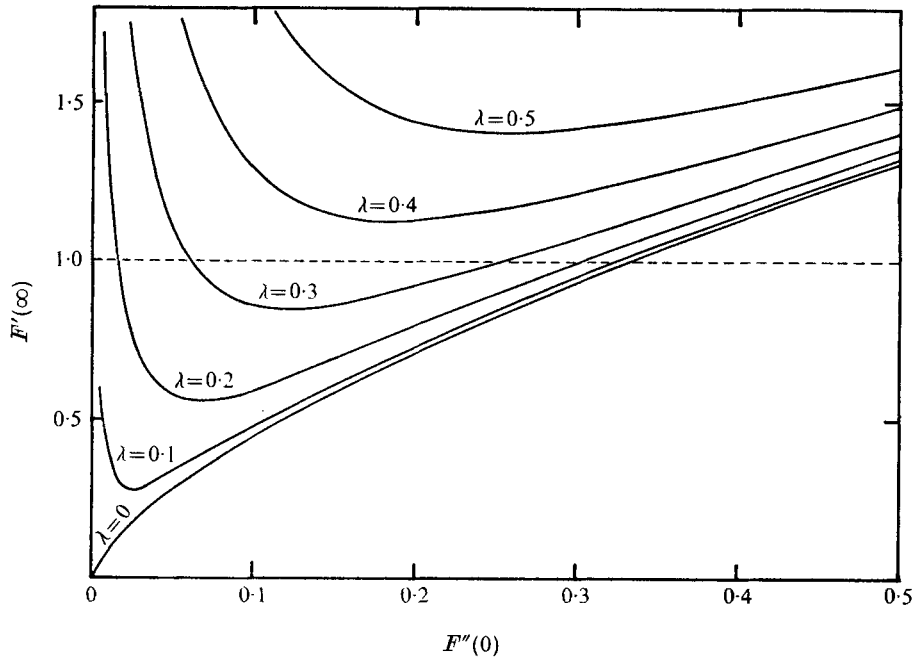


FIGURE 3. The solution of (1.1) as an initial-value problem.

thickness increases without bound as $\lambda \to 0$. In some respects, therefore, this second solution is analogous to the additional solution to the Falkner–Skan equation found by Stewartson (1954) when the wedge-angle parameter $\beta$ lies in the range $-0{\cdot}1988 < \beta < 0$, since as $\beta \to 0^-$ this additional solution does not converge to the Blasius function and its associated boundary-layer thickness becomes infinite. One interesting difference between the two cases, however, is that, at $\beta = -0{\cdot}1988$, where the two branches of the solutions to the Falkner–Skan equation merge, the wall shear stress vanishes, whereas in the present problem $F''(0)$ is still positive when $\lambda = \lambda^*$.

To illustrate further the nature of these two solutions for a given $\lambda$, we present in figure 4 plots of the corresponding tangential velocity and shear stress profiles, proportional to $F'(\eta)$ and $F''(\eta)$ respectively, for $\lambda = 0{\cdot}3$. As can be seen, in each case $F'(\eta)$ increases monotonically across the boundary layer while $F''(\eta)$ reaches a maximum at that value of $\eta$ where the stream function vanishes, i.e. along the line of contact between the recirculating flow and the external stream. The solution having a lower wall shear stress is characterized, however, by a substantially larger boundary-layer thickness which, as mentioned above, increases without bound as $\lambda \to 0$.

An attempt was also made to obtain the steady-state flow field for the moving-wall boundary-layer problem using as conditions at $x = 0$ and at $t = 0$ in (2.3) and (2.4) respectively the function $F'(\eta)$ from the second solution of (1.1) referred to above. Interestingly enough, the resulting flow structure converged to that found earlier except, of course, at $x = 0$, where it was required to conform to

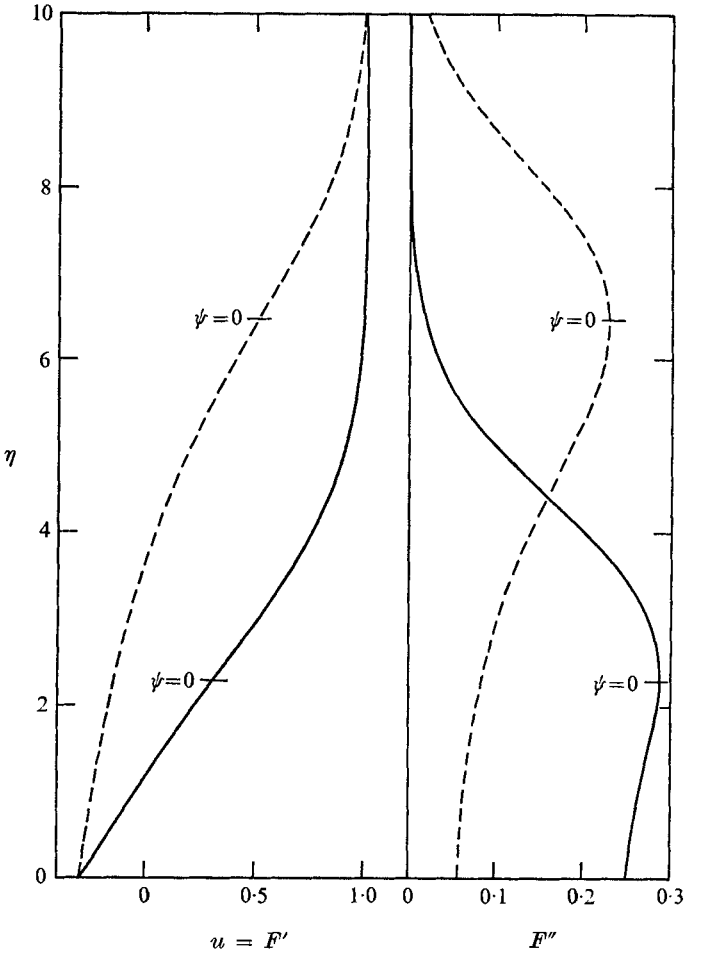


FIGURE 4. The two solutions of (1·1) for $\lambda = 0{\cdot}3$. ——, the solution obtained in I; – – –, the new (parasitic) solution.

the second solution of (1.1). Thus it would appear that his second solution is in some sense parasitic in that only the first solution, i.e. the one considered in I, with the larger wall shear stress and the smaller boundary-layer thickness, correctly describes the flow pattern near the leading edge of a finite flat plate.

At any rate, it is quite clear from figure 3 that (1.1) can have no solution for $\lambda > \lambda^*$ and $F''(0) \geqslant 0$.

## 4. The structure of the flow for $\lambda > \lambda^*$

It is instructive at this stage to examine briefly the possibility that the flow for $\lambda > \lambda^*$ could still be determined using only the boundary-layer equations but with the point of detachment $x_s$ located ahead of the leading edge. At first glance, this line of inquiry appears promising because, as mentioned in § 1, it would seem

logical to suppose that, when $\lambda$ becomes large, the reverse flow will carry enough momentum to be able to penetrate into the region upstream of the plate and thereby cause the surface streamline $\psi = 0$ to detach at $x_s < 0$. Nevertheless, it quickly becomes apparent that this possibility has to be abandoned since an analysis of the boundary-layer equations near the point of detachment $x = x_s$ reveals that the transformation (2.1) will still apply, with $\eta \equiv Y/(x-x_s)^{\frac{1}{2}}$, and that, as $x \to x_s$, the function $F$ will still satisfy (1.1) but with boundary conditions $F(0) = 0$, $F''(0) = 0$ and $F'(\infty) = 1$. Clearly, $F'(\eta) \equiv 1$ is the only solution of such a system. We conclude, therefore, that when $\lambda > \lambda^*$ the region where the reverse flow first comes into contact with the mainstream must assume a structure which can no longer be described on the basis of the boundary-layer equations.

In view of the above, we are led to propose a flow pattern which consists basically of three regions: the undisturbed stream ahead of the point of detachment $x = x_s$, a boundary layer similar to that discussed in §2 for $x > x_s$, and, separating the two, a collision region in the neighbourhood of $x_s$ within which the reverse flow turns around sharply and then moves downstream. In this collision region, whose structure is sketched in figure 5, the lateral and longitudinal length scales are both $O(R^{-\frac{1}{2}})$ – this is necessary if the solution downstream of the collision region is to match with that in the boundary layer – and hence the motion is here inviscid with vorticity being conserved along each streamline. Specifically, with $\psi$ the stream function, $\omega(\psi)$ the vorticity, $X \equiv R^{\frac{1}{2}}(x-x_s)$ and, as before, $Y \equiv R^{\frac{1}{2}}y$, we have that

$$\nabla^2\psi = -\omega(\psi), \tag{4.1}$$

where $\omega(\psi)$ is the vorticity of the fluid as it enters this collison region from its surrounding boundaries.† Of course, since the uniform stream is irrotational, $\omega \equiv 0$ for $\psi > 0$, while for $\psi < 0$ the vorticity can be obtained by differentiation from $u(x_s, Y, t) \equiv -u_c(Y, t)$, which, as shown in figure 5, refers to the longitudinal velocity component of the reverse flow near $x_s$, i.e. within that portion of the overlap domain between the boundary layer and the collision region where $u \leqslant 0$. Thus, if $u_c(Y, t)$ is known from the solution of the boundary-layer equations for $x > x_s$, $\omega(\psi)$ is everywhere specified and (4.1) can be solved in principle. Fortunately though, as will be seen, a solution of (4.1), which would be difficult to obtain owing to its nonlinearity, is not required for the purposes of this first-order analysis.

We now establish a useful result which follows immediately from the fact that, as $X \to \infty$, the solution to (4.1) must match with that in the boundary layer, i.e. as $X \to \infty$, the streamlines in the $X$, $Y$ plane must become horizontal. Therefore if, as shown in figure 5, $Y_1$ refers to the location of the $u = 0$ curve (or the curve of minimum $\psi$) as $x \to x_s^+$, we see from (4.1) and the condition $\partial\psi/\partial Y = 0$ at $Y = Y_1$ that, as $X \to \infty$, $\psi$ becomes an even function of $Y - Y_1$ for $0 \leqslant Y \leqslant 2Y_1$ and linear in Y for $Y > 2Y_1$. Hence we conclude that, in the overlap domain

† It can easily be shown that, to $O(R^{-\frac{1}{2}})$, the flow within the collision region can be assumed steady even if the flow in the boundary layer is time dependent.

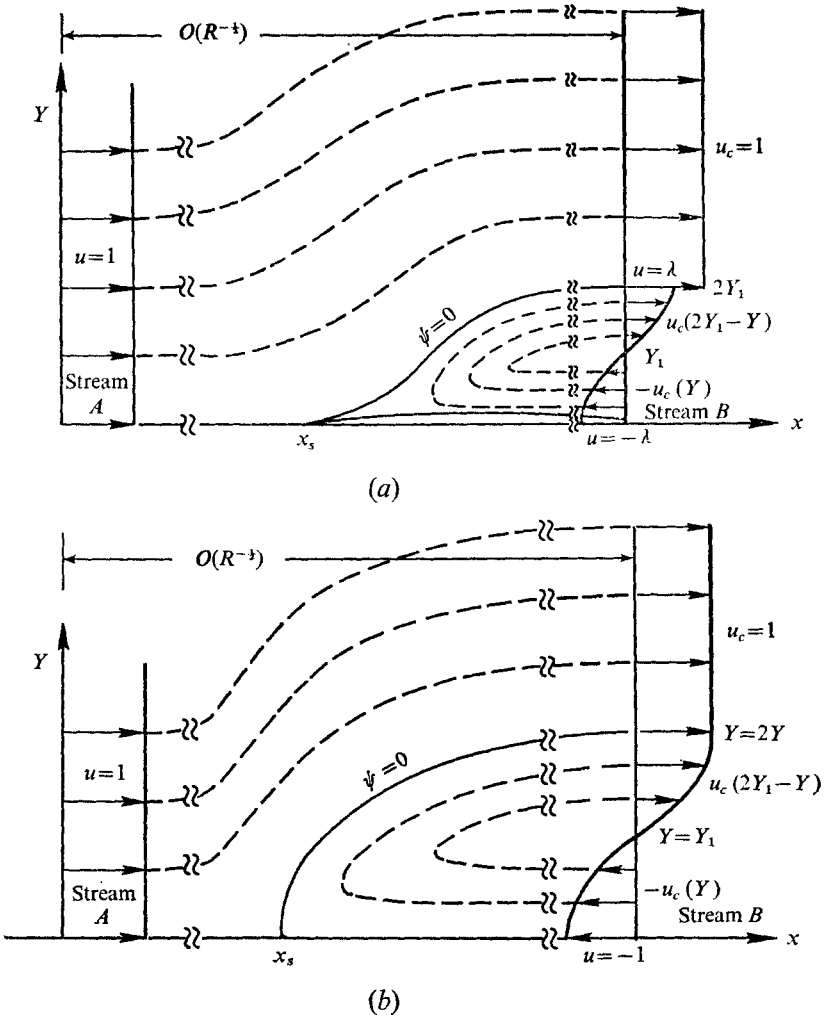


FIGURE 5. The flow structure in the collision region.
(*a*) $0{\cdot}3541 < \lambda < 1$. (*b*) $1 < \lambda < \infty$.

between the collision region and the boundary layer, $u$ must be odd in $Y-Y_1$ for $0 \leqslant Y \leqslant 2Y_1$ and uniform for $Y > 2Y_1$, i.e.

$$u(x_s, Y, t) = \begin{cases} -u_c(Y,t), & 0 \leqslant Y \leqslant Y_1, \\ u_c(2Y_1 - Y, t), & Y_1 \leqslant Y \leqslant 2Y_1, \\ 1, & Y \geqslant 2Y_1, \end{cases} \tag{4.2}$$

which will then serve as the appropriate boundary condition for the solution of the boundary-layer equation for $x > x_s$. By using the boundary conditions (4.2), as outlined above, solutions to the boundary-layer equations valid downstream of $x_s$ can then be obtained without solving for the flow within the inviscid collision region. Evidently, however, it is not possible to locate the point $x_s$ uniquely solely on the basis of the foregoing analysis, because one could assume in principle

any value $x_s \leqslant 0$ within some reasonable range and then compute a seemingly respectable solution valid downstream of that point. This indeterminacy must of course be resolved before meaningful numerical solutions can be obtained and hence certain features of the flow within the collision region will first be studied in detail in order to derive the appropriate criteria for locating the point of detachment $x_s$.

To this end, let us consider the collision between two inviscid streams $A$ and $B$, and in particular the local solution of the inviscid flow equation near $x_s$, the point of bifurcation of the $\psi = 0$ streamline (cf. figures 5*a*, *b*). In what follows, we shall suppose that at upstream infinity stream $A$ has a uniform velocity $u_A = 1$ in the $x$ direction, while at downstream infinity the corresponding velocity components of stream $B$ are

$$u_B = -\gamma + \omega_0 y, \quad v = 0, \tag{4.3}$$

where $\gamma$ and $\omega_0$ are constant non-negative parameters. Also, the undisturbed pressure of both streams is taken to be zero. Thus stream $A$ is everywhere irrotational while $B$ has a constant vorticity equal to $-\omega_0$. We wish to determine the necessary conditions for the existence of a steady solution to the inviscid equations in the neighbourhood of $x_s$; this requires, of course, that the pressure be continuous along the streamline $\psi = 0$ separating the two streams.

It is easily seen, first of all, that near $x_s$, the origin of our co-ordinate system, the streamline $\psi = 0$ will be either vertical, as in figure 5(*b*), or have the form of a cusp $Y \sim X^\alpha$, with $\alpha > 1$, as in figure 5(*a*). The remaining possibility, a wedge of finite angle, can immediately be eliminated because $x_s$ is then a stagnation point for both streams and the pressure variation along $\psi = 0$ will be always different for $A$ and $B$ no matter what the value of the wedge angle and of $\omega_0$. To determine, however, which of the two possibilities, i.e. a vertical line or a cusp, applies, it is necessary to consider separately the cases $\omega_0 = 0$ and $\omega_0 > 0$.

*Case* 1: $\omega_0 = 0$. Here, the flow depicted in figure 5(*b*) is certainly possible, but only if $\gamma = 1$ since $x_s$ is a stagnation point for both streams. As for the possibility of the streamline $\psi = 0$ being a cusp near $x_s$, this can be eliminated by the following argument.

Let us consider the local solution of Laplace's equation $\nabla^2\psi = 0$ for $X > 0$ and $0 < Y < X^\alpha$ ($\alpha > 1$) satisfying the boundary conditions $\psi = 0$ at $Y = 0$ and at $Y = X^\alpha$. We seek a solution of the form

$$\psi = H(X) \sin \pi Y / X^\alpha, \tag{4.4}$$

where by substitution we have that, to first order as $X \to 0$,

$$X^2 H'' - \pi^2 X^{2(1-\alpha)} H = 0.$$

The solution of the above which vanishes as $X \to 0$ is

$$H = X^{\frac{1}{2}} K_{1/2(\alpha-1)}\left(\frac{\pi}{(\alpha-1)\, X^{\alpha-1}}\right),$$

$K$ being a modified Bessel function of the second kind. Thus, as $X \to 0$, and noting that $\alpha > 1$,

$$H \to \left(\frac{2}{\pi}\right)^{\frac{1}{2}} X^{\frac{1}{2}\alpha} \exp\left\{-\frac{\pi}{\alpha-1}\, X^{1-\alpha}\right\}, \tag{4.5}$$

which shows that the velocity vanishes exponentially inside the cusp. In contrast, as will be seen below in (4.10), the speed along the top side of the $\psi = 0$ streamline, i.e. the part in contact with stream $A$, varies algebraically and hence a pressure match across the dividing streamline cannot be achieved under these conditions.

We conclude therefore that, as was to be expected, a steady flow pattern can result from the collision of two uniform streams only if both have the same speed.

*Case* 2: $\omega_0 > 0$. Again, the flow shown in figure 5 (*b*) is possible but this requires that, once more, $\gamma = 1$. In contrast to the previous case, however, it will be shown that a steady flow can exist for $\gamma < 1$ with the dividing streamline being a cusp.

To begin with, we note that, for $0 < Y < X^\alpha$, the appropriate equation is now $\nabla^2\psi = \omega_0$, which as $X \to 0$ has the particular solution

$$\psi = -\tfrac{1}{2}\omega_0\{YX^\alpha - Y^2\} \tag{4.6}$$

in addition to (4.4) and (4.5). Thus we have to first order as $X \to 0$ that $q_B$, the speed of stream $B$ along the $\psi = 0$ streamline, is

$$q_B = \tfrac{1}{2}\omega_0 X^\alpha, \tag{4.7}$$

plus an exponentially small term arising from the homogeneous solution (4.5).

On the other hand, for stream $A$, which is irrotational, we need to solve Laplace's equation subject to the conditions

$$v = \alpha u X^{\alpha-1} \quad \text{at} \quad Y = X^\alpha \quad (X \geqslant 0), \quad v = 0 \quad \text{at} \quad Y = 0 \quad (X < 0). \tag{4.8a,b}$$

However, to a first approximation we can impose (4.8*a*) on the $+X$ axis, rather than at $Y = X^\alpha$. Thus, on using complex-variable theory, we readily obtain

$$u - iv = a_0 + a_1(-z)^{\alpha-1} + \ldots, \quad z \equiv X + iY, \tag{4.9}$$

$a_0$ and $a_1$ being constants. It follows then that

$$u = a_0 + a_1(-X)^{\alpha-1} + \ldots, \quad v = 0 \text{ on the negative real axis,}$$

$$u = a_0 + a_1 X^{\alpha-1}\cos(\alpha-1)\pi + \ldots, \quad v = -a_1 X^{\alpha-1}\sin(\alpha-1)\pi + \ldots$$

on the positive real axis,

where, in view of (4.8),

$$a_1 = -a_0\,\alpha/\sin(\alpha-1)\pi.$$

The above ceases to apply when $\alpha$ is an integer, in which case $z^{\alpha-1}$ is to be replaced by $z^{\alpha-1}\ln z$ and the constant $a_1$ re-evaluated.

When $\alpha$ is not an integer then, we obtain for $q_A$, the speed of stream $A$ along the dividing streamline,

$$q_A = a_0\{1 - \alpha X^{\alpha-1}\cot(\alpha-1)\pi + \ldots\}. \tag{4.10}$$

But, in view of Bernoulli's equation, continuity of pressure across the $\psi = 0$ streamline requires that

$$q_A^2 - q_B^2 = 1 - \gamma^2, \tag{4.11}$$

which, on account of (4.7), can be satisfied only if

$$a_0 = (1-\gamma^2)^{\frac{1}{2}}, \quad \text{i.e. } \gamma \leqslant 1, \quad \text{and if} \quad \alpha = \tfrac{3}{2}, \tfrac{5}{2}, \ldots, \text{ etc.}$$

Higher-order terms in the solution can be obtained in a straightforward manner by expanding (4.8$a$) in a Taylor series about $Y = 0$. Thus, when $\alpha = \frac{3}{2}$ for example, the velocity of stream $A$ is given by

$$u - iv = a + a_1(-z)^{\frac{1}{2}} + a_2(-z) + a_3(-z)^{\frac{3}{2}} + \ldots,$$

while the equation for the dividing streamline is

$$Y = X^{\frac{3}{2}}(1 + b_1 X + b_2 X^2 + \ldots). \tag{4.12}$$

Substitution of the above in (4.8) with the higher-order terms included, as well as in (4.7) and (4.11), then leads to

$$a_0 = (1-\gamma^2)^{\frac{1}{2}}, \quad a_1 = -\tfrac{3}{2}(1-\gamma^2)^{\frac{1}{2}}, \quad a_2 = \tfrac{15}{8}(1-\gamma^2)^{\frac{1}{2}}, \quad a_3 = \tfrac{5}{2}b_1 - \tfrac{39}{16}(1-\gamma^2)^{\frac{1}{2}} \text{ etc.},$$

with similar results for $\alpha = \frac{5}{2}, \frac{7}{2}$, etc. Thus we see that, if $\gamma \leqslant 1$, local solutions can be constructed which, as expected, will contain many parameters, e.g. the $b_k$'s in (4.12), whose value can only be obtained from the overall solution to the problem. Of course, it is not clear at this stage of the analysis whether, in fact, an infinite number of possible local solutions will exist, corresponding to $\alpha = \frac{3}{2}, \frac{5}{2}$, etc., or whether a single $\alpha$ can be selected from this set with $\alpha = \frac{3}{2}$ being the most probable choice, but this will not affect the conclusions that follow.

Although admittedly incomplete in many respects, the arguments presented above lead to a criterion for locating $x_s$, the point of detachment of the $\psi = 0$ streamline in the moving-boundary problem, to which we shall now return.

Let us suppose first of all that $x_s < 0$. In this case, the reverse flow near the line of symmetry $Y = 0$ has zero vorticity owing to the boundary condition $(\partial u/\partial Y)_{Y=0}$ for $x < 0$, and hence the term $\omega_0$ in (4.3) is also zero. In view of the preceding discussion (case 1), a steady solution within the collision region is possible only if $\gamma \equiv u_c(0,t) = 1$. Consequently, since $u_c(0,t) < \lambda$ if $x_s < 0$, we can immediately conclude that detachment will occur ahead of the leading edge only if $\lambda > 1$, and that $x_s$ will be located at the point where the reverse-flow velocity along the line of symmetry $Y = 0$ has been decelerated to such an extent that $u_c(0,t) = 1$.

On the other hand, if $\lambda \leqslant 1$, $x_s$ will either coincide with or lie within an $O(R^{-\frac{1}{2}})$ distance from $x = 0$. In this case, $\gamma \equiv u_c(0,t) = \lambda < 1$ and $\omega_0 \equiv (\partial u_c/\partial Y)_{Y=0} > 0$, and hence the necessary conditions for the existence of a steady solution within the collision region (case 2) are satisfied. Of course, the flow structure within the collision region will now become rather complicated owing to the existence of a velocity discontinuity across the $\psi = 0$ streamline [cf. (4.11)], which in turn will require the presence of an $O(R^{-\frac{3}{4}})$ thick boundary layer along this detached streamline. Similarly, an $O(R^{-\frac{3}{4}})$ boundary layer will exist along $Y = 0$. These complications do not however affect the present first-order analysis.

## 5. Numerical solutions for $\lambda > \lambda^*$

In view of the results of the previous section, it is now possible to develop a solution to the boundary-layer equations for $\lambda > 0{\cdot}3541$ without having to solve for the flow field within the collision region. In fact, it is only necessary to alter,

at $x = x_s$, the numerical scheme described in §2, in order to account for the boundary conditions which result from the presence of the collision region.

To begin with we note that, in this range of $\lambda$, solutions will no longer have a similar form in the vicinity of $x_s$ and thus the boundary-layer equations are most conveniently solved in the conventional $x, Y$ framework. In dimensionless variables these equations have the familiar form

$$\left.\begin{aligned} \frac{\partial u}{\partial t} + u\frac{\partial u}{\partial x} + V\frac{\partial u}{\partial Y} &= \frac{\partial^2 u}{\partial Y^2}, \\ \partial u/\partial x + \partial V/\partial Y &= 0, \end{aligned}\right\} \tag{5.1}$$

where $V$ is the transverse velocity scaled by $R^{\frac{1}{2}}$. With $Y$ as the transverse co-ordinate in place of $\eta$, the numerical scheme outlined in §2 can be simplified since it is not necessary to use an implicit representation for terms containing $Y$ derivatives. The solution can then be explicitly stepped forward in time using the following finite-difference equations:

$$\left.\begin{aligned} \delta_{2t} u &= -u\delta_{2x} u - V\delta_{2Y} u + \delta_{YY} u, \\ \delta_Y V &= -\delta_{2x}\bar{u}^Y, \end{aligned}\right\} \tag{5.2}$$

where the finite-difference operators are defined by (2.7). Also, at the downstream boundary, $x$ derivatives are represented by one-sided differences with $\partial u/\partial x$ specified as in (2.8).

It is worthwhile to mention that, in the present explicit scheme, the magnitude of the time step that can be used is limited by the mesh size $\Delta x$, which is small compared with $\Delta Y$. Thus convergence to a steady-state solution could be accelerated by incorporating an implicit representation in the $x$ direction for (5.1). The numerical procedure would then be similar to the implicit scheme outlined in §2, the only difference being that the implicit direction would be switched from $\eta$ to $x$. Such an implicit formulation was not adopted here, however, since the computer time requirements for the explicit scheme were not excessive.

The integration of (5.2) begins by assuming that uniform flow exists throughout the domain at $t = 0$. Thus the initial and boundary conditions are

$$\left.\begin{aligned} &u(x, Y, 0) = 1, \quad V(x, Y, 0) = 0, \\ &u(x, 0, t) = -\lambda \text{ for } 0 \leqslant x \leqslant 1, \; \partial u(x, 0, t)/\partial Y = 0 \text{ for } x < 0, \; x > 1, \\ &V(x, 0, t) = 0, \quad u(x, \infty, t) = 1, \\ &u(x_s, Y, t) = \begin{cases} u_c(2Y_1 - Y, t), & Y_1 \leqslant Y \leqslant 2Y_1, \\ 1, & Y \geqslant 2Y_1, \end{cases} \end{aligned}\right\} \tag{5.3}$$

where, as discussed earlier, $u_c(Y, t)$ $(0 \leqslant Y \leqslant Y_1)$ is uniquely determined from the reverse flow entering the collision region between $Y = 0$ and $Y = Y_1$. The numerical procedures for obtaining $u_c$ are outlined below. We have already shown that, for $\lambda \leqslant 1$ and at steady state, this inviscid collison region must be located at the leading edge of the plate and consequently the domain of integration for the boundary-layer equations also begins at $x = x_s = 0$. Initially

$u(x_s, Y, 0) = 1$, the 'collision' region is not yet present, and (5.2) are stepped forward in time in the usual manner. After a time step has been completed, it is necessary to determine whether a collision region has been established or, if it is already present, how it has been altered during that time step. This in turn is determined by the nature of the region of reverse flow adjacent to the plate as $x \to x_s$. Thus, with reference to (4.2), the profile $u_c(Y,t) = -u(x_s, Y, t)\,(0 \leqslant Y \leqslant Y_1)$ at the new time level is derived by extrapolating the tangential velocity to $x = x_s$ using computed values at the first two grid points downstream of $x_s$. This procedure for generating $u_c(Y,t)$ begins at the plate and is continued for increasing $Y$ until a negative value of $u_c$ is encountered. (Of course, if the extrapolated $u_c$ at the first grid point above the leading edge of the plate is negative, no collision region exists and the boundary condition remains $u(x_s, Y, t) = 1$.) $Y_1$ is then computed by linearly interpolating between the last positive value of $u_c$ and the first negative one to locate the point where $u = 0$. Equation (4.2) is then used to determine $u(x_s, Y, t)$ for $Y > Y_1$.

When $\lambda > 1$, the collision region moves upstream until, as described earlier, $u_c(0,t) = 1$. In the numerical integration, $x_s$ is allowed to move upstream by altering the computational procedure in the following manner: after $u_c(Y,t)$ has been generated at $x = x_s$ at the new time level, the tangential velocity at $Y = 0$ is extrapolated one grid point further upstream by computing

$$u^* \equiv u(x_s - \Delta x, 0, t) = 2u(x_s, 0, t) - u(x_s + \Delta x, 0, t).$$

If $u^* < -1$, the extent of the integration domain is increased by adding an additional column of grid points one grid interval upstream of the present location of $x_s$. The numerical integration now requires the profile for $u_c(Y,t)$ at this new location for $x_s$, which is provided the first time simply by linearly extrapolating the entire column from downstream. It should be emphasized, of course, that the procedure adopted here is not meant to model accurately the transient behaviour of the collision region, but rather to devise a computationally efficient scheme for converging to a steady-state solution for the original moving-wall boundary-layer problem.

The techniques described above allow the inviscid collision region to change both its structure in $Y$ and its position in $x$ until a steady state is achieved which is consistent with the solution to the boundary-layer equations downstream of $x_s$. In generating these solutions, 61 grid points were used in the transverse direction and the thickness $L$ of the integration domain was held at $L = 6$ for $\lambda < 1$, but was increased to $L = 10$ for $\lambda > 1$ to account for the observed greater boundary-layer thicknesses. The time step and tangential grid size were specified in the same manner as described in §2 and the same small damping term was incorporated to maintain stability.

The steady-state streamline patterns obtained from the numerical solutions for $\lambda = 0{\cdot}5$ and $\lambda = 1{\cdot}0$ are presented in figures 6 (*a*) and (*b*). Here, only the closed-streamline regions adjacent to the plate are depicted, and the heavy solid line along the upstream edge of the region of closed streamlines denotes the location of the collision region. As $\lambda$ increases, the region of closed streamlines grows in thickness and the vortex centre moves upstream until at $\lambda = 1$ it has just reached

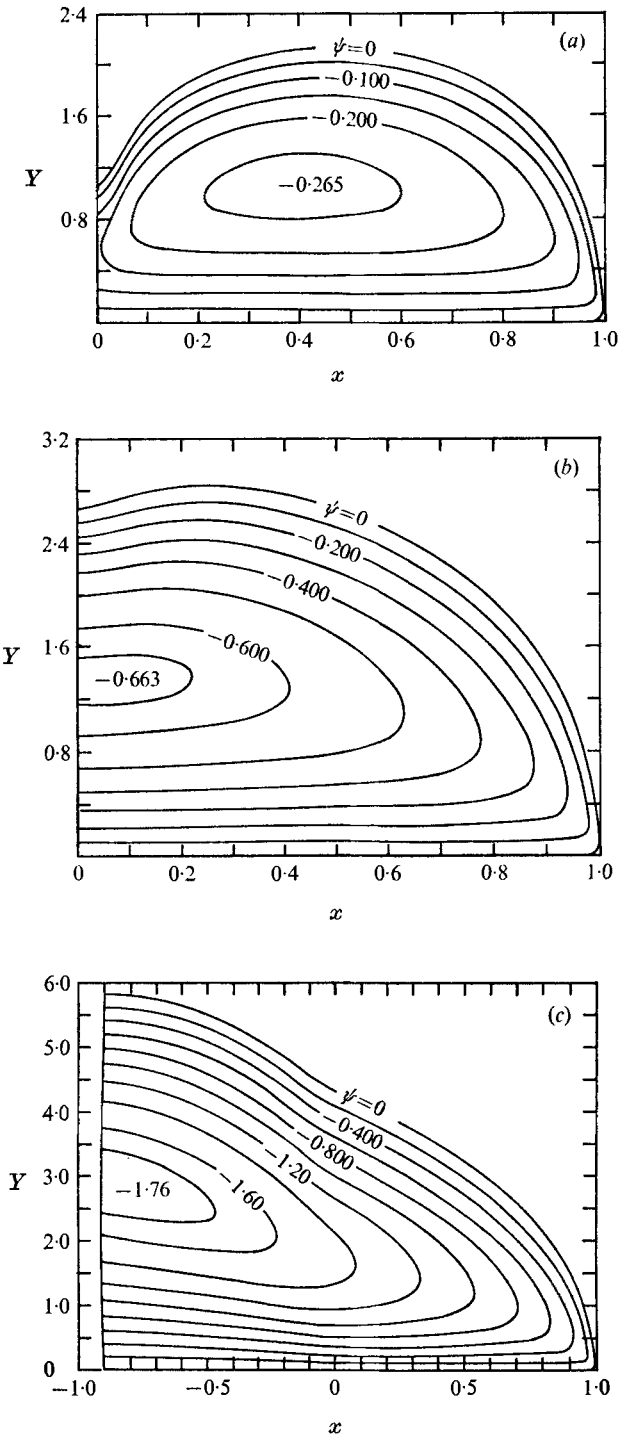


FIGURE 6. The structure of the closed-streamline region in the boundary layer when (*a*) $\lambda = 0{\cdot}5$, (*b*) $\lambda = 1{\cdot}0$ and (*c*) $\lambda = 2{\cdot}0$. In (*c*), $x_s = -0{\cdot}9$.

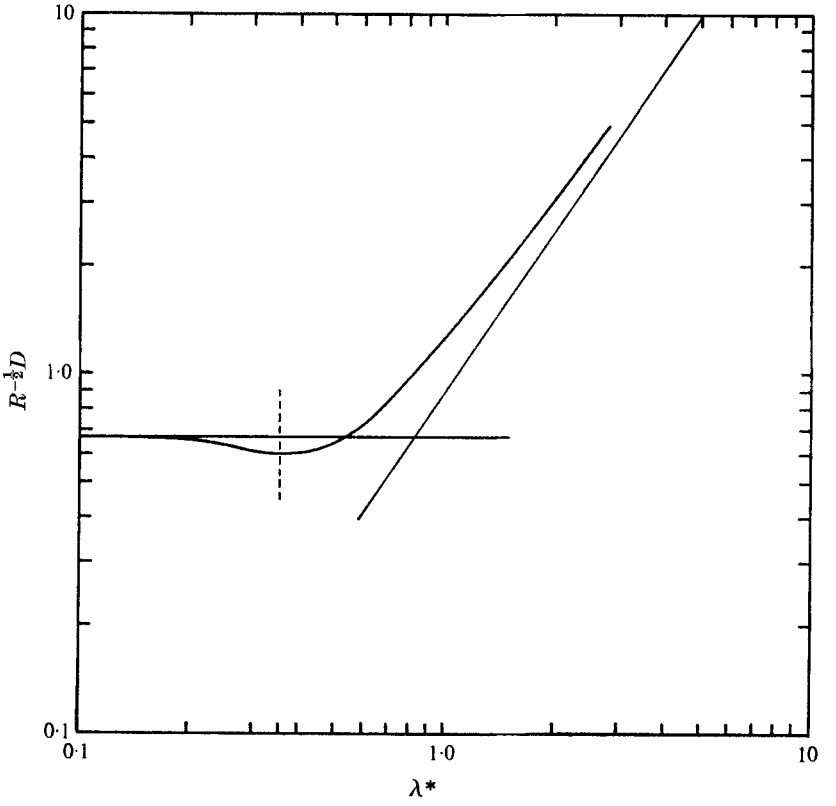


FIGURE 7. The dimensionless drag as a function of $\lambda$.

the leading edge of the plate, where the collision region is located. Also, as expected, the thickness of the collision region vanished within the accuracy of the numerical calculations as $\lambda \to \lambda^*$ from above.

As $\lambda$ is increased above unity, the point of detachment of the $\psi = 0$ streamline moves upstream of the leading edge of the plate and the vortex centre maintains its position adjacent to the collision region. To illustrate the flow structure in this regime, the closed-streamline region is plotted in figure 6(*c*) for $\lambda = 2$. Here $x_s = -0{\cdot}9$. Note that the region of closed streamlines increases in thickness more rapidly over that portion of the flow field which extends upstream from the leading edge, a result which can be anticipated by considering the limiting solution as $\lambda \to \infty$. In this case (which corresponds to $U \to 0$ with $\lambda U$ fixed), the boundary-layer equations have a similarity solution for $0 \leqslant x \leqslant 1$ in which the boundary-layer thickness grows in the upstream direction from the trailing edge $x = 1$ and is proportional to $(1-x)^{\frac{1}{2}}$ (Sakiadis 1960). Far upstream of the plate ($x < 0$), the flow again has a similar form which corresponds to the two-dimensional jet solution. Here the jet is created by the fluid forced upstream by the negative surface velocity, and the boundary-layer thickness becomes proportional to $(-x)^{\frac{2}{3}}$. Thus, for values of $\lambda$ in the range $1 < \lambda < \infty$, the separated bubble should grow more rapidly upstream of the plate than adjacent to it, and

for large values of $\lambda$, the recirculating region for $x < 0$ should thicken according to $(-x)^{\frac{3}{2}}$. As seen in figure 6(*c*), the solution for $\lambda = 2$ conforms qualitatively to this behaviour.

The dimensionless drag $R^{-\frac{1}{2}}D$ on the plate for the solutions with positive $\lambda$ is plotted in figure 7. As $\lambda$ increases from zero, the drag first decreases and then begins to increase for $\lambda > 0{\cdot}3541$. Reasons for the decrease in drag for $0 \leqslant \lambda \leqslant 0{\cdot}3541$ were presented in I. (The drag computed here for $0 < \lambda < 0{\cdot}3541$ is slightly different from that obtained in I, where it appeared that the drag began to increase when $\lambda$ exceeded a value of about 0·25. The earlier result was, however, influenced by a shear stress profile for $\lambda = 0{\cdot}3$, shown in figure 5 of I, which was slightly in error.) The drag profile can be compared with the asymptotes for $\lambda \to 0$ and $\lambda \to \infty$, which are also included in figure 7. As $\lambda \to 0$ the drag is given by the Blasius solution as 0·664, while for $\lambda \to \infty$ it becomes $0{\cdot}89\lambda^{\frac{3}{2}}$. Evidently, for $\lambda = 2$, the value of the drag is already close to that given by the asymptotic solution for $\lambda \gg 1$.

The solutions presented above provide a consistent description of the boundary-layer flow structure in the range $\lambda^* < \lambda < \infty$, where previously even a qualitative understanding of its features had been lacking. Here, the flow field differs from that of a conventional boundary layer in that an inviscid collision region is present in the vicinity of the point of detachment in which the reverse boundary-layer flow is turned in the direction of the mainstream. These solutions, together with those of §2, describe then the flow over the entire range $0 < \lambda < \infty$ for the moving-wall boundary-layer problem under consideration.

This research was supported in part by National Science Foundation grant ENG-74-23229 to Stanford University; the National Center for Atmospheric Research is sponsored by the National Science Foundation.

## REFERENCES

ELVIUS, E. & SUNDSTRÖM, A. 1973 Computationally efficient scheme and boundary conditions for fine mesh barotropic model based on the shallow water equations. *Tellus*, **25**, 132.

KLEMP, J. B. & ACRIVOS, A. 1972 A method for integrating the boundary-layer equations through a region of reverse flow. *J. Fluid Mech.* **53**, 177.

LEAL, L. G. & ACRIVOS, A. 1969 Structure of steady closed streamline flows within a boundary layer. *Phys. Fluids Suppl.* **2**, 105.

ROBILLARD, L. 1971 On a series solution for the laminar boundary layer on a moving wall. *Trans. A.S.M.E.* E **38**, 550.

SAKIADIS, B. C. 1960 Boundary-layer behavior on continuous solid surfaces: II. The boundary-layer on a continuous flat surface. *A.I.Ch.E. J.* **7**, 221.

STEWARTSON, K. 1954 Further solutions of the Falkner–Skan equation. *Proc. Camb. Phil. Soc.* **50**, 454.